ACADEMIC PRESS

Available online at www.sciencedirect.com
SCIENCE DIRECT®

Journal of Catalysis 218 (2003) 104–110

JOURNAL OF CATALYSIS

www.elsevier.com/locate/jcat

Mg–V–Al mixed oxides with mesoporous properties using layered double hydroxides as precursors: catalytic behavior for the process of ethylbenzene dehydrogenation to styrene under a carbon dioxide flow

Gabriela Carja,[a,*] Ryuichi Nakamura,[b] Takashi Aida,[b] and Hiroo Niiyama [b]

[a] *Department of Physical Chemistry, Faculty of Industrial Chemistry, Technical University of Iasi, 71 D. Mangeron, Iasi, Romania*
[b] *Department of Chemical Engineering, Tokyo Institute of Technology 2-12-1, O-okayama, Meguro-ku, Tokyo 152-8550, Japan*

Received 17 October 2002; revised 24 January 2003; accepted 24 January 2003

Abstract

A new catalyst for the process of ethylbenzene dehydrogenation to styrene under a CO_2 atmosphere was obtained using vanadium-substituted layered double hydroxides as precursors. After calcination, vanadium-substituted hydrotalcite-like samples gave mixed oxides with a high surface area and strong mesoporous characteristics; the XRD analysis indicates the formation of $Mg_3V_2O_8$ and $Mg_2Al_2O_4$ in bulk while the XPS results point to the presence of a mixture of V^{5+} and V^{3+} ions on the surface. Catalytic tests show that the styrene yield and selectivity increase when the vanadium content of the sample increases. The higher catalytic activity is attributed to the formation of V^{5+} on the surface that is promoted by the presence of CO_2 as a cofeed gas. The FTIR adsorption of pyridine shows that aluminum contributes to Lewis-type acidity of the catalyst and is important for establishing features of the catalyst deactivation process.

Keywords: Vanadium mixed oxides; Ethylbenzene dehydrogenation; Layered double hydroxide; CO_2 as promoter

1. Introduction

Hydrotalcite-like compounds or more generally speaking layered double hydroxides (LDHs) have the general formula $[M(II)_{1-x}M(III)_x \cdot (OH)_2]^{x+}(A^{n-}) \cdot mH_2O$ and belong to the class of anionic clays. Their structure consists of positively charged brucite-like $Mg(OH)_2$ layers wherein octahedra of Mg^{2+} cations share edges to form infinite sheets that are stacked on top of each other and held together by hydrogen bonds. When part of Mg^{2+} is substituted by M^{3+} cations the excess of the positive charge resulting from this substitution is counterbalanced by exchangeable anions A^{n-} located, as water molecules, in the interlayer space [1]. Thermal decomposition of hydrotalcite-like materials around 723 K gives a stable, high surface area, homogeneous and highly dispersed mixed metal oxides with active acid–base sites. Moreover, the incorporation of cations with redox properties in the LDH network offers the opportunity of designing new bifunctional mixed oxides with a unique combination of acid–base and redox properties [1,2].

Styrene, an important basic chemical as a raw material for polymers, is produced commercially by the dehydrogenation of ethylbenzene (EB) using a typical Fe–K–Cr oxide-based catalyst in the presence of a large quantity of steam [3]. For the actual industrial process a large amount of wasted energy in the form of excess steam, the thermodynamic equilibrium limitations, and the deactivation of catalyst are several problems which must be solved. In this context, recently, a new process of ethylbenzene dehydrogenation using as a cofeed gas CO_2 instead of steam has received much attention [4,5]. Mamedov and Corberan [6] explained the main role of CO_2 in the catalytic dehydrogenation process as follow:

- The hydrogen produced is removed as water by the reverse water gas shift reaction; therefore, the equilibrium limitation of dehydrogenation shifts to the products side.
- Carbon dioxide removes the deposited coke.

Using this information, to our knowledge for the first time, we tested, mixed oxides derived from vanadium-

* Corresponding author.
E-mail address: carja@uaic.ro (G. Carja).

0021-9517/03/$ – see front matter
doi:10.1016/S0021-9517(03)00051-4

substituted MgAl hydrotalcite as catalysts for the process of ethylbenzene dehydrogenation when carbon dioxide is used as a cofeed gas. Vanadium-containing catalysts were already tested in the catalytic process of EB dehydrogenation: Organowski et al. [7] reported that a high styrene yield and a good selectivity were obtained using V–Mg–O catalysts with an excess amount of steam and oxygen. Sakurai et al. reported the dehydrogenation of EB over vanadium loaded on activated carbon [8] and vanadium oxide loaded MgO [9] under a carbon dioxide atmosphere; recently it was also reported that vanadia–alumina catalysts exhibit high catalytic activity and selectivity for this process when carbon dioxide is present in the flow [10].

In this report we present the effects of vanadium incorporation in the LDH network on the porous and surface properties of the derived Mg–V–Al mixed oxides and also the preliminary results of the catalytic behavior of the characterized samples for the catalytic process of ethylbenzene dehydrogenation to styrene when CO_2 is used as a cofeed gas.

2. Experimental

2.1. Catalyst preparation

All the samples were synthesized following a coprecipitation method similar to that described by Reichle et al. [11], at a constant pH, under a bubbling constant flow of nitrogen in the reaction medium and vigorous stirring. Magnesium, aluminum nitrates, and vanadium chloride, in the desired molar ratio, were used as precursors and $NaOH/Na_2CO_3$ as precipitants. The obtained precipitates were separated by centrifugation, washed extensively with warm deionized water until they were sodium and chloride free and dried under vacuum at 338 K.

2.1.1. MgAlLDH

One hundred milliliters of an aqueous solution of $Mg(NO_3)_2 \cdot 6H_2O$ (0.02 mol)/$Al(NO_3)_3 \cdot 9H_2O$ (0.01 mol) and an aqueous solution of $NaOH/Na_2CO_3$ were added dropwise together, in such a way that the pH remained at a constant value of 9.5. The resulting white precipitate was aged at 338 K for 24 h under stirring.

2.1.2. VLDH

An aqueous solution (85 ml) of $Mg(NO_3)_2 \cdot 6H_2O$ (0.02 mol)/$Al(NO_3)_3 \cdot 9H_2O$ (0.01 mol-q)/VCl_3 (q mol, $0.003 \leqslant q < 0.01$) and an aqueous solution of Na_2CO_3 (1 M), were added dropwise together, over a period of 2 h, at a constant pH value of 8.9. The resulting white-gray precipitates were aged at 358 K for 24 h under a nitrogen atmosphere and stirring.

2.2. Characterization

2.2.1. XRF

The chemical compositions of synthesized samples were determined by X-ray fluorescence spectroscopy (Shimadzu XRF-1700 sequential X-ray fluorescence spectrometer).

2.2.2. XRD

X-ray powder diffraction patterns were recorded on a Philips PW 1840 diffractometer using monochromatic Cu-K_α radiation ($\lambda = 0.154$ nm), operating at 40 kV and 30 mA over a 2θ range from 4 to 70°.

2.2.3. N_2 adsorption at 77 K

N_2 adsorption isotherms were measured on a Coulter SA 3100 automated gas adsorption system. Prior to the measurements the samples were heated for 5 h under vacuum at 383 K in order to expel the interlayer water molecules. Microcomputer processing controlled the analysis. The BET specific surface area (S_{BET}) was calculated by using the standard Brunauer–Emmett–Teller method on the basis of adsorption data [12]. Pore-size distributions were calculated from the desorption branches of the isotherms using the Barret–Joiyner–Halenda method [13] and the corrected Kelvin equation. Pore volume values were determined by using the t-plot method of De Boer [14].

2.2.4. X-ray photoelectron spectroscopy (XPS)

The spectra were recorded using a Perkin-Elmer Model 5500-MT (ESCA/MC/SAM) surface science instrument equipped with a magnesium anode (1253.6 eV) operating at 300 W, 15 kV, and 20 mA. Microcomputer processing controlled the spectra acquisition and handling. Samples were analyzed as powders dusted onto double-sided sticky tape in an analysis chamber typically operating at 1×10^{-9} Torr (1 Torr = 133.3 Pa). All binding energy values (BE (eV)) were determined with respect to the C 1s line (284.6 eV) of the carbon overlayer and the standard deviation of the peak position was within ±0.1 eV. The surface (XPS) concentration of each element, expressed as surface atomic ratios, was calculated from the corresponding peak areas using specific atomic sensitivity factors, with the integral subtraction of the background [15].

2.3. FTIR analysis

The FTIR adsorption spectra were recorded using a Shimadzu (Model 8100 A-standard) FTIR spectrophotometer. The applied range, acquisition, and resolution were 4000–4350 cm^{-1}, 36 scans, and 4.0 cm^{-1}, respectively. The self-supporting disk was activated in an in situ IR cell at 673 K, under He flow, evacuated at 673 K for 60 min, and then exposed to pyridine at 298 K. The desorption was done for 30 min at room temperature, 358, 478, and 523 K. The spectra were recorded at room temperature with the integral sub-

traction of the background corresponding to each temperature.

2.4. Catalytic tests

Catalytic tests were performed in a flowing reaction system, in the temperature range 673–873 K, under atmospheric pressure. Prior to the catalytic tests each sample was calcined under air, at 723 K, for 5 h ($MeLDH_c$). After calcination the sample ($m = 0.8$ g) was placed between inert quarts sand layers in a quartz tubular reactor (i.d. 8 mm) and pretreated under He from room temperature to 723 K at a heating rate of 5° per minute. From 723 K to the reaction temperature the catalyst was maintained under a stream of CO_2 and He. The EB was evaporated in a controlled evaporation system; the total flow rate was 50 ml/min, with 0.2% vol EB, a molar ratio $CO_2/EB = 15{:}1$, and He as a carrier gas. The effluent from the reactor was condensed in a trap externally cooled in an ice-water bath and analyzed by a gas chromatograph (Shimadzu GC-8A) and FID equipped with a methyl silicon capillary column. Gaseous components were analyzed using an online TCD gas chromatograph.

Catalytic activity and selectivity of the tested samples were characterized by EB conversion value (X), styrene yield (YST), and styrene selectivity (SST). All the catalytic tests were carried out in duplicate; the results were reproducible within ±7%. Under these conditions the average was used for calculation and data analysis.

3. Results and discussion

The composition of the synthesized ternary hydrotalcites can be fully defined by the formula: $Mg_2V_xAl_{1-x}$ (atomic ratio: $Mg/V/Al = 2/x/(1-x)$). Therefore we will use the notation x VLDH to denote the composition of the substituted sample and to define the ternary sample name; we also will use the notation $x\text{VLD}_c$ for the samples calcined under air, at 723 K, 5 h. The chemical compositions and some structural properties of the synthesized samples are presented in Table 1. The Mg/V/Al atomic ratios determined by XRF are coincident, within experimental errors, with those of the starting mixed aqueous solutions. The XRD patterns (see Figs. 1a and 1b) with sharp and symmetric reflections for the *(003)*, *(006)*, *(110)*, and *(113)* planes and broad symmetric peaks for the *(102)*, *(105)*, and *(108)* planes

Table 1
Chemical composition and lattice parameters of MgAlLDH and VLDHs

Sample	Mg:Al:V	V (% mass)	XRD	Lattice parameters (Å)			IFS
		from XRF	phase	a	c	d_{003}	(Å)
MgAlLDH	2:1:0	0	LDH	3.053	23.34	7.8	3.0
0.5 VLDH	2:0.5:0.5	17.1	LDH	3.067	23.10	7.70	2.90
0.7 VLDH	2:0.3:0.7	22.0	LDH	3.089	22.83	7.61	2.81
VLDH	2: 0:1	27.0	LDH	3.097	22.74	7.57	2.77

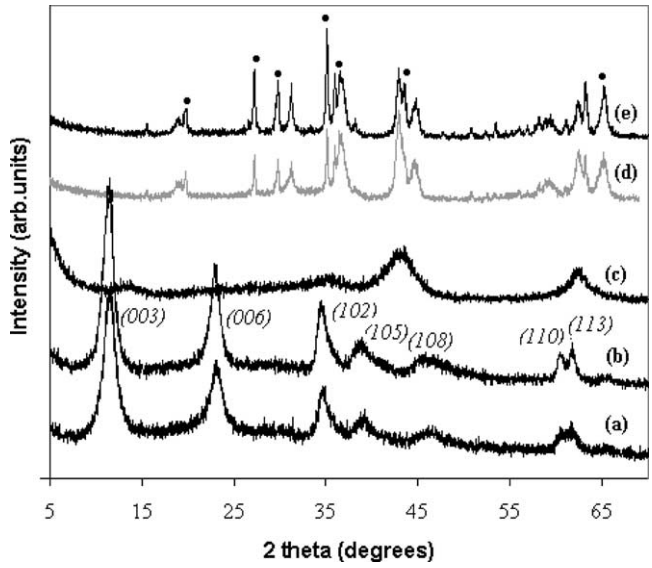

Fig. 1. XRD patterns of the characterized samples: (a) 0.7 VLDH hydrotalcite-like sample, (b) 0.5 VLDH hydrotalcite-like sample, (c) 0.5 VLDH sample after calcination at 723 K, (d) 0.5 VLDH after calcination at 1173 K, (e) 0.7 VLDH after calcination at 1173 K; •, $Mg_3V_2O_8$.

are characteristics of well-crystallized hydrotalcite-like materials [1]. The lattice parameters are calculated by indexing the peaks under a hexagonal crystal system, using a least-squares method; the parameter a corresponds to the cation–cation distance within the brucite-like layer while the parameter c is related to the total thickness of the brucite-like layer and the interlayer distance [1]. The increase of the parameter a for the vanadium-substituted samples clearly indicates that V^{3+} has replaced the Al^{3+} into the brucite-like layers, as the ionic radius of V^{3+} hexacoordinate is 0.64 Å (Shannon ionic radii [16]) whereas the ionic radius of Al^{3+} hexacoordinate is 0.53 Å (Shannon ionic radii [16]). The decrease of the parameter c and the d_{003} (basal spacing calculated from the 003 reflection position in the XRD pattern [1]) can be attributed to the modified electrostatic interactions between the layer and the interlayer network when another metal is introduced in the LDH layer [17]. The interlayer free spacing (IFS) values are calculated by subtracting the thickness of the LDH layer (4.8 Å) [1] from the calculated d_{003} spacing. The values decrease from 3.0 to 2.77 Å. The decrease in IFS value suggests a distortion of the LDH network induced in the substitution process of aluminum by vanadium.

Calcination of these materials at 723 K for 5 h leads to the destruction of the HT-like network giving rise to a diffuse amorphous pattern (see Fig. 1c) characteristic of the mixed oxides with poor crystallinity [1]. To follow the evolution of the obtained mixed oxides we analyzed the XRD patterns of the vanadium-substituted samples calcined at 1173 K for 5 h. The obtained patterns (Figs. 1d and 1e) are similar to those previously reported by Labajos et al. for the calcined LDHs containing V^{3+} in the layers. [18]; the diffraction peaks corresponding to mixtures of magnesium–vanadium mixed

Table 2
BET surface area and porosity characteristics of the calcined samples obtained from N_2 adsorption data

Sample	BET area (m^2/g)	V_p (ml/g)	%μpA	%mesopA
$MgAlLDH_c$	236.3	0.7320	23	77
0.5 $VLDH_c$	201	0.7630	17	83
0.7 $VLDH_c$	137.5	0.7710	12	88

oxides type $Mg_3V_2O_8$ (with V^V located in a tetrahedral oxide environment) and also $MgAl_2O_4$ are identified in the corresponding XRD patterns. Segregation of MgO, with the most intense (200) and (220) reflections ($2\theta \approx 64°$ and 44°, respectively) shifted toward higher angles in comparison to pure magnesia (JCPDS File No. 45-946), is also observed after calcination at this temperature. We also noted that the decrease of vanadium content gave a lower intensity of the characteristic reflections corresponding to $Mg_3V_2O_8$.

3.1. Textural characteristics

The values of BET surface area, the total pore volume (V_p), and also the extent of micropore area (%μpA) and mesopores area (%mesopA) in the total *t*-plot area of the calcined samples are presented in Table 2. After vanadium substitution the value of the BET surface area decreases while the pore volume value increases; the extent of area formed by mesopores in the total *t*-plot area is 77% for $MgAlLDH_c$ but increases to nearly 90% for the 0.7 $VLDH_c$ sample. The increasing contribution of mesopore area to the total *t*-plot area indicates that the decrease of the surface area is due to increased mesoporosity characteristics of the vanadium-substituted samples in comparison to $MgAlLDH_c$ samples. Fig. 2 presents the contribution of pores, as a function of their size range, to the total pore volume (calculated using pore-size distribution results). We can see that the pores in the range 5–20 nm contribute by nearly 55% to the total pore volume of $MgAlLDH_c$ while the contribution due to the pores with sizes between 20 and 40 nm is less than 20%. For 0.7 $VLDH_c$ almost 60% of the pore volume is due to the pores in the range 20–40 nm, though the pores in the range 5–20 nm contribute less than 26% to the total pore volume. These results indicate that the vanadium-containing mixed oxides possess increased mesoporous properties compared to the corresponding mixed oxides derived from MgAl hydrotalcite. It is already reported [19,20] that the alteration of the textural properties for the ternary-substituted LDHs is due to the modified microscopic morphology of the substituted samples.

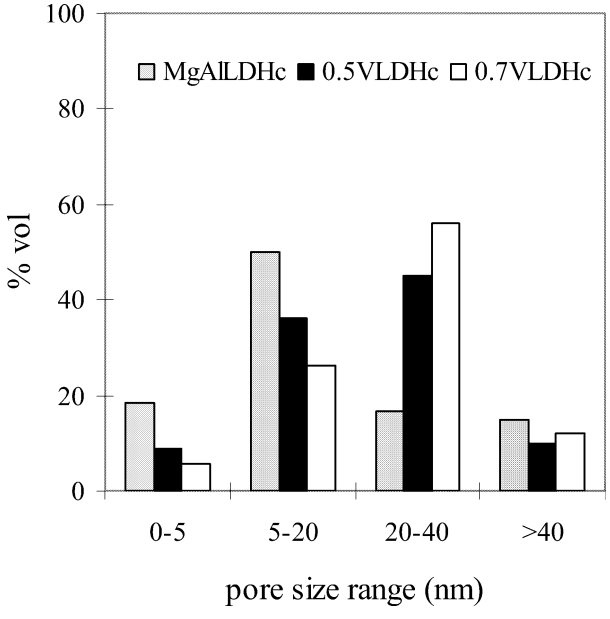

Fig. 2. Contribution of pores, as a function of their size range, to the total pore volume for $MgAlLDH_c$, 0.5 $VLDH_c$, and 0.7 $VLDH_c$.

3.2. XPS analysis

The nature of the active species present on the surface is important for establishing the properties of the catalytic samples. In this view the XPS analysis has been done in order to obtain information about the surface composition of the V–Mg–Al mixed oxides derived from vanadium-substituted hydrotalcite-like samples. The corresponding XPS spectra of $MgAlLDH_c$ and 0.7 $VLDH_c$ are shown in Figs. 3 and 4, respectively; the patterns are quite similar but some differences can be seen:

– For the vanadium-substituted sample a new peak appeared in the region of the spectrum corresponding to V $2p_{3/2}$ [21], indicating that vanadium is present on the surface of the sample. The peak (see Fig. 5a) is too broad to represent a single valency of the vanadium cation; in

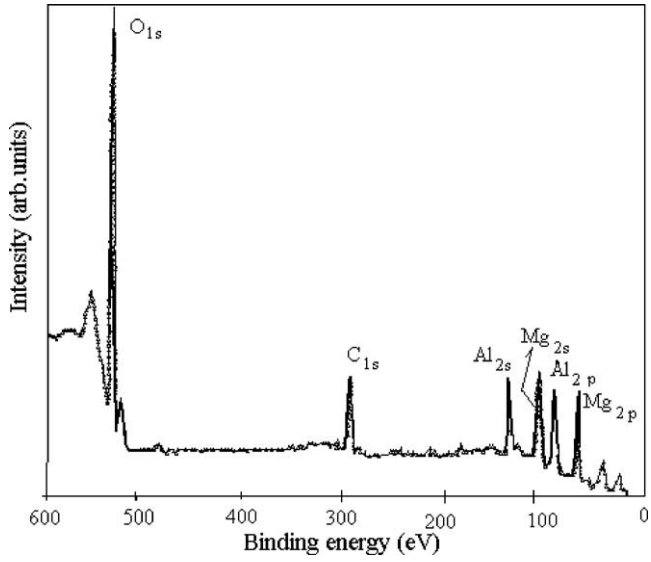

Fig. 3. XPS pattern of $MgAlLDH_c$.

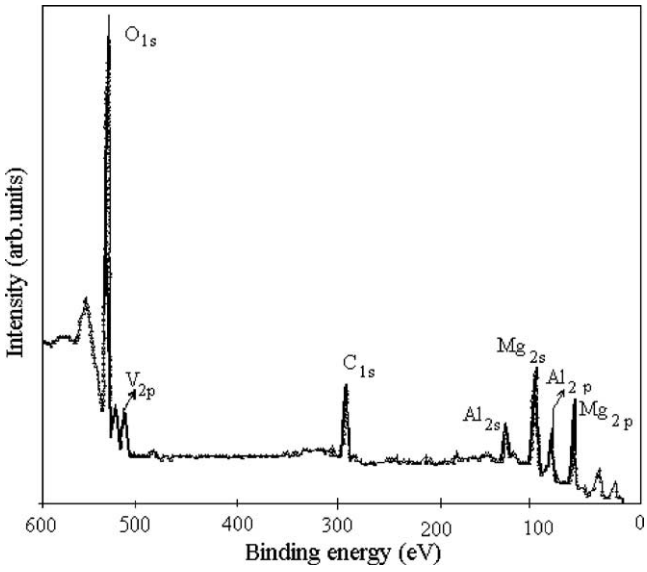

Fig. 4. XPS pattern of 0.7 $VLDH_c$.

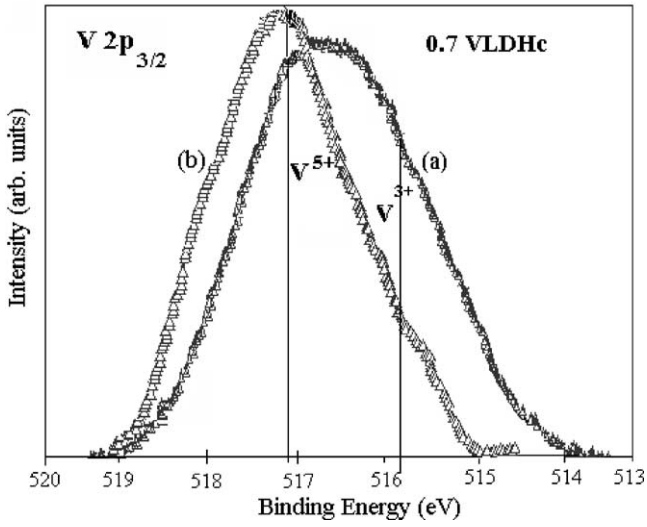

Fig. 5. V 2p XPS region in the corresponding XPS spectra of 0.7 $VLDH_c$. (a) Calcined sample at 723 K, (b) calcined sample at 723 K, after CO_2 treatment.

comparison to previous reported results [22] we can say that a mixture of vanadium ions including V^{5+}, with a maximum binding energy value at 517.2 eV [21,22], and also V^{3+}, with a maximum binding energy value at 515.8 eV [21,22], is detected by the XPS analysis on the surface of the vanadium-substituted sample.

In order to understand the effect of carbon dioxide on the catalyst surface we treated the 0.7 $VLDH_c$ fresh sample with carbon dioxide, at 823 K, for 2 h; the result of XPS analysis (see Fig. 5b) shows that the corresponding V $2p_{3/2}$ XPS region becomes narrower and is shifted to the left pointing out that after CO_2 treatment V^{5+} is mainly detected on the surface of the sample.

– There is no considerable shift in the binding energy value of Mg 2p centered at 49.65 ± 0.1 eV; however, the corresponding FWHM value increases from 2.12 eV for $MgAlLDH_c$ to 2.33 eV for 0.7 $VLDH_c$ pointing out a different environment for magnesium in vanadium-containing mixed oxides.
– A shift to a higher binding energy value of the O 1s peak from 530.5 eV for $MgAlLDH_c$ to 531.8 eV for 0.7 $VLDH_c$ is also observed. Such a shift was previously reported for Co-substituted hydrotalcite and it is assigned to oxygen from the nonstoichiometric spinel-type phase [23].

The surface (XPS) concentrations (expressed as percentage of surface atomic ratio) are presented in Table 3. The modification of the surface concentrations for all the elements suggests that the catalyst surfaces underwent reorganization after vanadium substitution. The surface concentrations of vanadium show lower values than the corresponding bulk concentrations while the surface concentrations of magnesium and aluminum point out the enrichment of magnesium and aluminum on the surface (such phenomena were previously reported [23,24] for other mixed oxides derived from substituted LDHs). The oxygen concentrations on the surface increase by 12% for 0.7 $VLDH_c$. In the condition the XRD analysis points out that $Mg_3V_2O_8$ is formed for the calcined vanadium containing LDHs, the fact that low $(V/Mg)_{XPS}$ ratios are obtained should indicate [25] the presence of isolated VO_4 tetrahedra on the sample surface.

For the used catalyst the surface concentration of vanadium is very low, the surface concentration of oxygen also decreases, and a preferential segregation of aluminum on the surface is observed. The variations of the surface concentrations after reaction point to the direct involvement of the species present on the surface in the catalytic process.

Table 3
Surface atomic ratios (%) of XPS-detected elements for the catalytic tested samples

Sample	Surface atomic ratio (%)					
	Oxygen	Aluminum	Magnesium	Vanadium	V/Mg	V/Al
$MgAlLDH_c$	51.7	17.9	30.4	–	–	–
0.7 $VLDH_c$	64.3	9.2	22.8	3.7	0.16 (0.33)[a]	0.40 (2.33)[a]
$VLDH_c$	67.7	–	27.4	4.9	0.17	–
0.7 $VLDH_c$ used catalyst	54.6	20.5	24.4	0.4	0.016	0.02

[a] Bulk value from XRF.

Table 4
Dehydrogenation of EB to styrene with (a) CO_2 as a cofeed gas and (b) in the absence of CO_2 in the feed, over mixed oxides derived from hydrotalcite-like samples[a]

Sample	X (%)	YST (%)	SST (%)
	(a)		
$MgAlLDH_c$	21.4	14.2	78.9
0.5 $VLDH_c$	36.7	33.4	87.1
0.7 $VLDH_c$	51.8	46.9	92.9
$VLDH_c$	54.6	49.7	94.7
	(b)		
$MgAlLDH_c$	19.2	12.5	75.1
0.5 $VLDH_c$	23.8	19.1	84.4
0.7 $VLDH_c$	27.5	24.7	91.7
$VLDH_c$	33.2	29.7	92.4

[a] At 808 K, under standard reaction conditions, after 1 h on stream.

3.3. Catalytic activity in the process of ethylbenzene dehydrogenation

Table 4 summarizes the catalytic tests results for the process of ethylbenzene dehydrogenation to styrene at 808 K, after 1 h on stream and standard reaction conditions when CO_2 is used as a cofeed gas (Table 4a) and in the absence of CO_2 in the flow (Table 4b). We note that the higher the vanadium content of the tested sample the higher the catalytic activity in the process of styrene formation. In the presence of CO_2 the ethylbenzene conversion reaches 55% for $VLDH_c$ though the value decreases to nearly 50% for the 0.7 $VLDH_c$; for the $MgAlLDH_c$ sample the conversion of EB is only 21.4%. The obtained styrene yield is equal to 14% for $MgAlLDH_c$, though the value increases to nearly 46% for 0.7 $VLDH_c$ and to 50% for $VLDH_c$. All the vanadium-containing samples are highly selective to styrene reaching a maximum equal to nearly 95%. On the other hand, in the absence of CO_2 (under He flow), the values of styrene yield and ethylbenzene conversion decrease and a maximum value of styrene yield equal to nearly 30% is obtained for $VLDH_c$ sample. Fig. 6 shows the obtained ethylbenzene conversion, styrene yield, and styrene selectivity versus reaction temperature for the 0.7 $VLDH_c$ sample. The dependence of EB conversion and styrene yield on temperature is nearly linear; a minimum styrene yield equal to nearly 12% is obtained at 673 K while a maximum value of 63.3% is reached at 873 K. Styrene selectivity decreases from 95% at 673 K to 90% at 823 K. The absence of CO_2 in the flow led to an important decrease of the styrene yield with a maximum equal to 27.7% at 823 K. We also tested the catalytic behavior of the sample 0.7 $VLDH_c$ after reduction under H_2, at 833 K, for 2 h; the catalytic activity (with CO_2 in the flow) decreases dramatically and a styrene yield value equal to nearly 27% was obtained at 808 K. This result together with the XPS analysis of the sample pretreated with CO_2 underlines that V^{5+} is the active catalytic site for the process of ethylbenzene dehydrogenation. This result is an agreement with the result of Sakurai et al. [9] and points out the role of CO_2 to promote the studied catalytic process by oxidizing V^{3+} to V^{5+}. A qualitative comparison of the obtained results with the results previously reported for vanadium oxide-loaded MgO [9] and alumina-supported vanadia [10] catalysts shows that Mg–V–Al mixed oxides derived from substituted LDH possess good catalytic properties for the process of ethylbenzene dehydrogenation to styrene under a CO_2 flow.

The features of the deactivation process for ethylbenzene dehydrogenation to styrene are influenced by the presence of aluminum. Fig. 7 presents the variation of styrene yield as a function of time on stream at a temperature equal to 873 K. The sample $VLDH_c$ is characterized by a styrene yield equal to nearly 70% after 1 h of catalytic run, though the value decreases to nearly 20% after 7 h. The loss of styrene yield

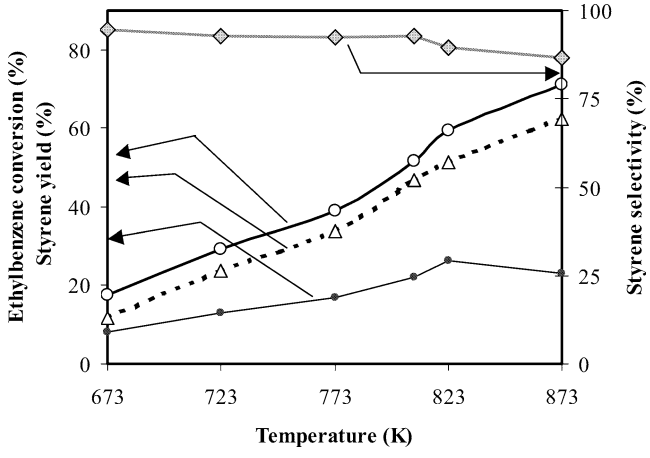

Fig. 6. Effect of the reaction temperature on ethylbenzene conversion (○), styrene yield (△), and styrene selectivity (◇), in the presence of CO_2 in the flow and styrene yield (●) in the absence of CO_2 in the flow, after 1 h on stream and standard reaction conditions for 0.7 $VLDH_c$ catalytic sample.

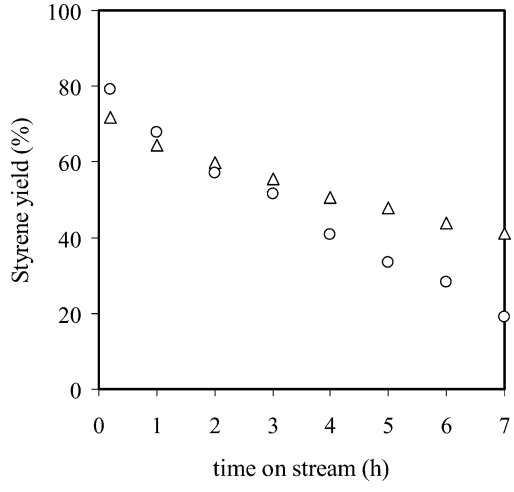

Fig. 7. Effect of time on stream on the styrene yield. Experimental conditions: reaction temperature 873 K, CO_2/EB molar ratio, 15:1; and $W/F = 16$ g_{cat} h/mol_{EB} for (△) 0.7 VLD_c and (○) VLD_c catalytic samples.

(LYST), calculated using the formula:

$$\big(\mathrm{YST}(1\ \mathrm{h}) - \mathrm{YST}(7\ \mathrm{h})\big) \cdot 100/\mathrm{YST}(1\ \mathrm{h}) = \mathrm{LYST},$$

is equal to 70%. For 0.7 $VLDH_c$ the initial value of the styrene yield is equal to 64% after 1 h on stream but the LYST value decreases to 40%. These results show that the increase of the vanadium content assures higher values for the initial styrene yield and selectivity but the presence of aluminum reduces catalyst deactivation. To explain the influence of aluminum on the catalyst deactivation process we studied the differences of the acidity features of $VLDH_c$, 0.7 $VLDH_c$, and 0.5 $VLDH_c$. For this reason we used the pyridine adsorption IR spectroscopy to differentiate between the different surface site types of the tested samples. The pyridine adsorption on supported vanadium oxides has been discussed thoroughly in the literature [26,27]. The bands at 1610, 1576, 1490, and 1466 cm^{-1} have been assigned to the vibrational modes of Lewis acid sites coordinated Py while the bands at 1640, 1576, 1490, and 1538 cm^{-1} were assigned to both Brønsted and Lewis acid sites. In our study, the same adsorption bands characteristic of pyridine on Lewis and Brønsted sites were observed for all the catalysts; also no significant shift of the peak positions was observed. To compare the acidity of the samples we used the main peaks situated at ~ 1490 cm^{-1} (Lewis acidic site peak—LPy) and at ~ 1544 cm^{-1}, respectively (Brønsted acidic sites peak—BPy). The areas under these peaks (after desorption at 358 K) were used for a quantitative comparison for the number of the acid sites of the tested samples [28]. The obtained results point out that the contribution of Brønsted acidity to the total acidity of the catalysts is low emphasized for all the samples, though it increases when the vanadium content increases. Aluminum contributes to increasing the number of Lewis acid centers; therefore, we can say that the presence of aluminum accentuates the Lewis acidity characteristics of the tested samples. This result shows that the weak acidic sites (Lewis type) could have a significant contribution in preventing catalyst deactivation. While CO_2 plays a key role in the formation of the active catalytic site, V^{5+}, the weak acidic sites induced by the presence of aluminum contribute to reduce the catalyst deactivation.

4. Conclusions

Using vanadium-substituted hydrotalcites as precursors we synthesized vanadium-containing mixed oxides with strong mesoporous characteristics and high surface area. The hydrotalcite-like structure gave, after calcination, a special environment for the vanadium ions in the bulk and also on the surface of the samples. All these features contribute to establish high values of the styrene yield and selectivity when these samples were tested as catalysts for the process of EB dehydrogenation to styrene when CO_2 is used as a cofeed gas. Both redox and acidic properties of the derived vanadium-substituted layered double hydroxides influence the catalytic process characteristics.

Acknowledgments

G.C. gratefully acknowledges financial support from the Ministry of Education of Japan for a research fellowship at Tokyo Institute of Technology. We thank Dr. Y. Kameshima for assisting in the XPS measurements and Prof. K. Okada for the hospitality of his laboratory.

References

[1] F. Cavani, F. Trifiro, A. Vaccari, Catal. Today 11 (1991) 173, and references therein.
[2] A. Vaccari, Appl. Clay Sci. 14 (1999) 161.
[3] E.H. Lee, Catal. Rev. Eng. Sci. 8 (1973) 285.
[4] M. Nimura, M. Saito, Catal. Lett. 58 (1999) 59.
[5] M. Sugino, H. Shimada, T. Turuda, H. Miura, N. Ikenaga, T. Suzuki, Appl. Catal. A 121 (1995) 125.
[6] E.A. Mamedov, V.C. Corberan, Appl. Catal. A 127 (1995) 1.
[7] W. Organowski, J. Hanuza, L. Kepinski, Appl. Catal. A 171 (1998) 145.
[8] Y. Sakurai, T. Suzaki, N. Ikenaga, T. Suzuki, Appl. Catal. A 192 (2000) 281.
[9] Y. Sakurai, T. Suzaki, K. Nakagawa, N. Ikenaga, H. Aota, T. Suzuki, J. Catal. 209 (2002) 16.
[10] V.P. Vislovskiy, J.S. Chang, M.S. Park, E.S. Park, Catal. Commun. 3 (2002) 227.
[11] W.T. Reichle, S.Y. Yang, S.D. Everhardt, J. Catal. 10 (1986) 352.
[12] S. Brunauer, P.H. Emmett, E. Teller, J. Am. Chem. Soc. 60 (1938) 309.
[13] E.P. Barret, L.J. Joiyner, P.P. Halenda, J. Am. Chem. Soc. 73 (1953) 373.
[14] S.J. Gregg, K.S.W. Sing, Adsorption, Surface Area and Porosity, 2nd ed., Academic Press, London, 1982.
[15] C. Deffose, in: F. Dellany (Ed.), Chemical Industries, Vol. 15, Dekker, New York, 1984, p. 225.
[16] R.D. Shannon, Acta Crystallogr. A 32 (1976) 751.
[17] S. Velu, N. Shah, T.M. Jyothi, S. Sivansaker, Micropor. Mesopor. Mater. 33 (1999) 61.
[18] F.M. Labajos, V. Rives, P. Malet, M.A. Centeno, M.A. Ulibarri, Inorg. Chem. 35 (1996) 1154.
[19] G. Carja, R. Nakamura, T. Aida, H. Niiyama, Micropor. Mesopor. Mater. 47 (2001) 275.
[20] F. Malherbe, C. Forano, J.P. Besse, Micropor. Mater. 10 (1997) 67.
[21] C.D. Wagner, W.N. Riggs, L.E. Davis, G.F. Moulder, G.E. Muilenberg (Eds.), Handbook of X-ray Photoelectron Spectrometry, Perkin–Elmer, Eden Praine, MN, 1979.
[22] M. Demeter, M. Neuman, W. Reichelt, Surf. Sci. 454–456 (2000) 41.
[23] S. Kannan, C.S. Swamy, Catal. Today 53 (1999) 725.
[24] G. Carja, R. Nakamura, H. Niiyama, Appl. Catal. A 236 (2002) 91.
[25] A. Corma, J.M. Lopez Nieto, N. Paredes, J. Catal. 144 (1993) 425.
[26] F. Hatayama, T. Ohno, T. Maruoka, T. Ono, H. Miyata, J. Chem. Soc., Faraday Trans. 92 (1996) 1401.
[27] T. Blasco, A. Galli, J. Lopez Nieto, F. Trifiro, J. Catal. 169 (1997) 203.
[28] M. Amiridis, R. Duevel, I. Wachs, Appl. Catal. B 20 (1999) 111.